

## Article

# Fluvial Response to Environmental Change in Sub-Tropical Australia over the Past 220 Ka

Jacky Croke <sup>1,\*</sup> , Chris Thompson <sup>2</sup>, Annegret Larsen <sup>3</sup> , Mark Macklin <sup>4</sup> and Kate Hughes <sup>1</sup>

<sup>1</sup> School of Earth and Atmospheric Sciences, Queensland University of Technology, Brisbane 4000, Australia; kate.hughes@qut.edu.au

<sup>2</sup> Seqwater, Spring Hill 4305, Australia; chris.thompson@seqwater.com.au

<sup>3</sup> School of Environmental Sciences, Wageningen University and Research, 6708 PB Wageningen, The Netherlands; annegret.larsen@wur.nl

<sup>4</sup> Department of Geography, University of Lincoln, Lincoln LN6 7TS, UK; mmacklin@lincoln.ac.uk

\* Correspondence: jacky.croke@qut.edu.au; Tel.: +61-731380181

**Abstract:** This paper uses a 30 m record of valley alluviation in the Lockyer Creek, a major tributary of the mid-Brisbane River in Southeast Queensland, to document the timing and nature of Quaternary fluvial response. A combination of radiocarbon and optically stimulated luminescence dating reveals a sequence of major cut and fill episodes. The earliest aggradation phase is represented by a basal gravel unit, dating to ~220 ka (marine isotope sub-stage 7d), and although little evidence supports higher fluvial discharges during MIS 5, a MIS 3 fluvial episode characterised by incision and aggradation dates to ~60 ka. A penultimate phase of incision to a depth of 30 m prior to ~14 ka saw the lower Lockyer occupy its current position within the valley floor. The Lockyer Creek shows evidence of only minor fluvial activity during MIS 2, suggesting a drier LGM climate. The appearance of alternating fine- and coarse-grained units at about 2 ka is notable and may represent higher-energy flood conditions associated with a strengthening of El Niño Southern Oscillation activity as observed in the flood of 2011. The aggradation rate for this Holocene floodplain unit is ~11 times higher than the long-term rate.

**Keywords:** valley fill; luminescence dating; avulsion; Southeast Queensland; base level; climate change; flood



**Citation:** Croke, J.; Thompson, C.; Larsen, A.; Macklin, M.; Hughes, K. Fluvial Response to Environmental Change in Sub-Tropical Australia over the Past 220 Ka. *Quaternary* **2024**, *7*, 9. <https://doi.org/10.3390/quat7010009>

Academic Editors: Xianyan Wang, Jef Vandenberghe, Ping Wang and David Bridgland

Received: 14 December 2023

Revised: 2 February 2024

Accepted: 6 February 2024

Published: 9 February 2024



**Copyright:** © 2024 by the authors. Licensee MDPI, Basel, Switzerland. This article is an open access article distributed under the terms and conditions of the Creative Commons Attribution (CC BY) license (<https://creativecommons.org/licenses/by/4.0/>).

## 1. Introduction

Our knowledge of global Quaternary climate change and fluvial dynamics has been significantly improved by reconstructing historical river activity from alluvial sequences [1,2]. Alluvial systems have the ability to document the history of climate change through sedimentary signals and sequences. Additionally, they may adapt to climatic changes by modifying sediment movement and geomorphological features, such as channel diameters, rates of change, and patterns [3].

In the geologically stable region of eastern Australia, climate is commonly seen as the main element controlling the response of rivers across the period of Quaternary glacial/interglacial cycles [4]. Not many studies go back as far as the last glacial/interglacial cycle, and the current interpretations are still heavily affected by reconstructions of past climates from the dry interior. These reconstructions have been utilised to emphasise the alternating periods of increased and decreased moisture on the continent [5]. Nevertheless, this pattern of alternating periods of wetting/activity and drying/inactivity is expected to have overestimated, or at least not fully captured, the significant amount of climate fluctuations that occur both within and between specific glacial and interglacial cycles [6].

Our understanding of river response to these climate changes remains inconsistent and limited to select regions in Australia. Within the channels of the Riverine Plain in New South Wales, there is a well-documented record of changes during the late Quaternary

period [7–10]. These data show that the channels have generally been smaller and less sinuous, which is consistent with the continent being drier. In different settings, the major response has been terrace aggradation and incision [11], although it is still not well known to what degree these represent external or internal controls [12,13].

The main objectives of our study on the valley fills of the Lockyer Creek, an important tributary of the Brisbane River in Southeast Queensland (SEQ), are the following: (1) to understand the historical changes in the valley's river system from the early Pleistocene to late Holocene; (2) to examine the sedimentary sequences in the valley fills and establish a timeline to identify periods of incision and aggradation in the river, and (3) to investigate the relationship between these changes and climate, as well as potential internal factors. The data presented here offer the initial chance to study this phenomenon in a river system located in the sub-tropical region of Australia, a region which has received limited focus in terms of longer-term Quaternary paleoclimate reconstructions.

### Regional Setting

The Lockyer Creek (~3000 km<sup>2</sup>) is a sub-catchment of the Brisbane River in eastern Australia and discharges into Moreton Bay (Figure 1a).

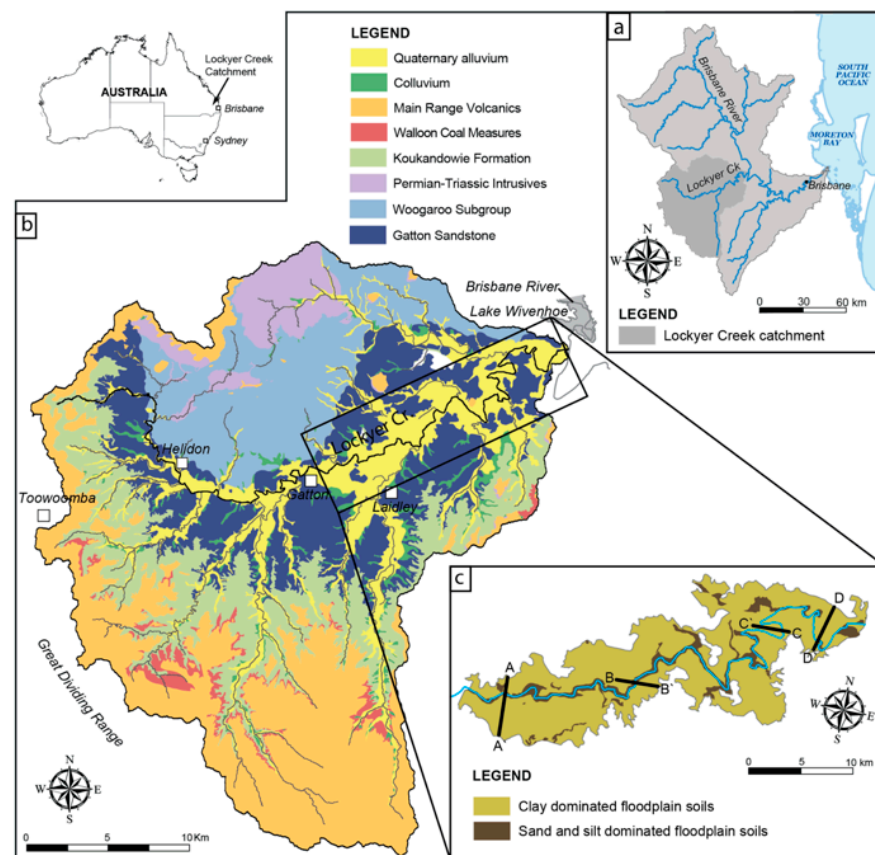


**Figure 1.** (a) Location of Southeast Queensland and the tributaries of the Brisbane catchment with its outlet at Moreton Bay. (b) The Lockyer Valley with mapped geological units consisting of the Tertiary Basalt and Jurassic Walloon coal measures; the Jurassic Marbourg Formation consisting of the Koulandowie and Gatton Sandstone formations. The lower Jurassic Koukandowie Formation is the upper unit, and the Gatton Sandstone is the basal unit of the Marburg Subgroup, respectively. (c) Inset of the lower Lockyer showing the distribution of selected groundwater log transects and differentiation of the clay and silty/sand-dominated floodplains after Powell (1987) [14].

Quaternary terrace and floodplain alluvium deposits border the main channel of the Lockyer Creek to the mid-Brisbane River confluence (Figure 1b) at an elevation of ~24 m AHD. Tertiary basalt and Jurassic Walloon coal measures make up the catchment geology

on the divide, while the headwaters have incised into and flow over the Jurassic Marburg Formation, which is made up of Koulandowie and Gatton Sandstone Formation (Figure 1b). The lower Lockyer Valley, characterised by expansive alluvial plains, primarily comprises black and brown cracking clays and gradational clay loams. This region is renowned for its very productive horticulture industry in Australia [14].

The climate is described as subtropical, with average maximum monthly temperatures fluctuating between 21 and 29 °C. The yearly precipitation fluctuates from 900 to 1800 mm, with the majority occurring during the warm summer season (October to February) [15]. The region is distinguished by fluctuating patterns of floods and droughts that have been associated with the year-to-year changes in rainfall caused by the El Niño–Southern Oscillation (ENSO) and the Interdecadal Pacific Oscillation (IPO) [16]. On 10 January 2011, a severe rainfall storm caused flash floods in the upper catchment area, leading to a major loss of life and changes in the landscape [17].

The lower Lockyer Creek is defined here as the main channel from Gatton, down to the confluence with the mid-Brisbane River (Figure 1c). The main channel alternates between low sinuosity reaches and tight meandering bends which abutt bedrock and other confining media. The channel geometry of the lower Lockyer is variable but persistently large, with bankfull discharge > 10-year recurrence interval [17]. Natural levees occur on both banks until 16 km from the confluence [18]. Since European settlement in the late 1800s, two-thirds of the native vegetation has been cleared for agricultural purposes [19].

## 2. Materials and Methods

The Queensland groundwater database provided 6944 bore records for the Lockyer catchment, out of which 2330 recorded the depth-to-bedrock specifically along the valley bottom [20]. A single database was utilised to create a 3D geological model and a potentiometric surface map of the valley [20]. The bedrock longitudinal profile was derived by interpolating data from the bedrock digital elevation model (DEM), with the distance upstream standardised to match the existing length of the Lockyer Creek thalweg. The basal gravel layer on top of the bedrock was estimated as the highest level of gravel deposition before periods of erosion, as confirmed by optically stimulated luminescence (OSL) dating and drilled at two cross-sections (A, B in Figure 1c). The floodplain surface profile is determined by the mean height of the top of the river banks, which is obtained from the 2013 lidar-derived digital elevation model (DEM). The 2010 lidar-derived digital elevation model (DEM), obtained when there was minimal water flow, was utilised to extract the current channel thalweg heights. The weir pools were eliminated from the long profile by employing linear interpolation between the channel bed sites located upstream and downstream.

The groundwater bore logs revealed the presence of a bedrock ‘palaeovalley’ with a width of approximately 2 to 3 km and a depth of around 15 to 30 metres (as shown in cross-section A in Figure 2).

A Geoprobe 6610DT drill rig was used to drill two valley cross-sections, which constitute nine cores and were chosen as representative of the diverse bedrock topography. Due to the considerable thickness of the sediment deposited in the valley (>25 m) and the laborious process of continuously extracting samples from compact, fine-grained alluvium, we prioritised dating the coarse layers using optically stimulated luminescence (OSL). The depth of valley fill was adjusted linearly for each core to account for sediment compression (e.g., sands) or expansion (e.g., clays).

The cores were dissected in the laboratory using a Geotek core splitter while being illuminated with red light. They were then thoroughly cleaned and examined to determine any changes caused by soil formation, the size of the grains, the presence of sedimentary structures, and the characteristics of the boundaries between different layers. The sediment less than 2 mm was examined using a Malvern Instruments Mastersizer 2000 laser diffractometer. Grain size categories were established based on standard measures [21] to determine the proportions of sand, silt, and clay. Samples with higher sand ratios were interpreted to

indicate higher energy, in-channel transportation, while samples with poorly sorted, silt, and clay-dominated deposits were associated with lower energy overbank deposition.

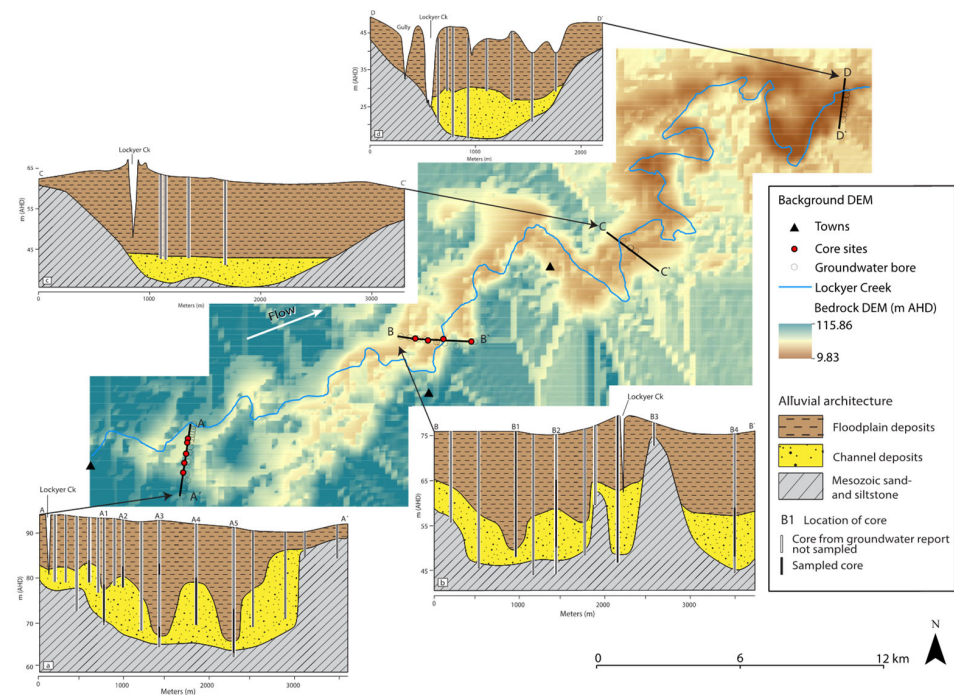


**Figure 2.** Bedrock DEM (m AHD) of the lower Lockyer to the confluence with the mid-Brisbane River. DEM derived from interpolation of groundwater bore logs of depth to bedrock to create a 90 m grid. Inset cross sections (A)–(D) selected from the groundwater database showing the geometry of major gravel, sand, and silty loam units.

### 2.1. OSL Dating

After the samples were pre-treated to eliminate carbonates, organics, feldspars, and heavy minerals, quartz sands with a size range of 180–220  $\mu\text{m}$  were subjected to etching in 48% hydrofluoric acid for a duration of 40 min. This process aimed to remove the outer 10  $\mu\text{m}$   $\alpha$ -irradiated rind. The Risø instrumentation was used to determine the values of the single-grain equivalent dose ( $D_e$ ). This was done by following the modified single aliquot-regenerative dose (SAR) protocol described in reference [22]. The protocol involved stimulating with infrared (IR) diodes before measuring the single-grain contamination of feldspar. For more information on the preheat testing and saturation test dose response, please refer to Figures S1 and S2. The acceptance/rejection criteria outlined in reference [23] were employed, whereby grains were deemed rejected if the sensitivity of either the second or third test dosage signals differed from that of the first test dose by more than 20%.

The age modelling approach developed by Galbraith and colleagues [24–26], including the unlogged variations [27], was used to determine the burial dosage ( $D_b$ ) for each population of single grain  $D_e$  values. This approach was chosen based on the presence of  $D_e$  values with uncertainties that intersect zero. A value of overdispersion ( $\sigma_d$ ) was calculated for each sample, where  $\sigma_d$  indicates the extent of variability in the data that cannot be accounted for by known sources of uncertainty (i.e., assigned measurement uncertainty on each individual single grain  $D_e$ ). A burial dose was computed using the central age model (CAM) when  $\sigma_d$  is low (<20%). This assumes that most grains were fully bleached before burial and that there may be some minor degree of over-dispersion. In cases when the  $\sigma_d$  exceeds 20%, the minimum age model (MAM) is employed, assuming that partial bleaching is the primary cause of the excessive dispersion. The CAM is deemed acceptable in cases when it is corroborated by other age models and approaches, particularly in samples exhibiting significant overdispersion. The conclusive burial of  $D_e$  and the corresponding age models employed are outlined in Table 1.

**Table 1.** OSL and radiocarbon sample information and age estimates.

Core	Lab ID	Field ID	<sup>238</sup> U (Bq/Kg)	<sup>226</sup> Ra (Bq/Kg)	<sup>210</sup> Pb (Bq/Kg)	<sup>228</sup> Ra (Bq/Kg)	<sup>228</sup> Th (Bq/Kg)	40K (Bq/Kg)	Dose Rate Total (Gy/Ka)	Estimated Dose (Gy)	Age (Ka)	† Age Model
A1	15-0210-054	L6-1-110	21 ± 6	18 ± 2	15 ± 5	27 ± 3	26 ± 2	286 ± 20	1.62 ± 0.13	112 ± 2.09	69.35 ± 5.56	a
	15-0210-055	L6-2-150	10 ± 4	7 ± 1	9 ± 3	12 ± 1	13 ± 1	110 ± 10	0.83 ± 0.07	118 ± 2.44	142.39 ± 11.74	a
	15-0210-057	L6-3-290	14 ± 5	14 ± 2	15 ± 4	16 ± 2	18 ± 2	132 ± 10	1.03 ± 0.09	231.4 ± 17.4	225.6 ± 25.4	a
A2	15-0210-059	L8-1-110	8 ± 8	14 ± 2	5 ± 7	15 ± 3	21 ± 2	362 ± 26	1.73 ± 0.13	20.8 ± 0.64	12.01 ± 0.96	a
	15-0210-060	L8-2-150	11 ± 5	11 ± 2	8 ± 4	15 ± 3	14 ± 2	253 ± 18	1.39 ± 0.11	36.74 ± 1.25	26.40 ± 2.21	a
	15-0210-062	L8-3-265	10 ± 3	8 ± 1	8 ± 3	10 ± 1	10 ± 1	203 ± 17	1.05 ± 0.08	29.62 ± 1.19	28.14 ± 2.37	a
	15-0210-066	L8-4-450	18 ± 8	17 ± 3	13 ± 7	14 ± 3	19 ± 2	299 ± 25	1.45 ± 0.11	61.96 ± 4.92	42.80 ± 4.77	a
A3	15-0210-067	L10-1-60	31 ± 10	19 ± 2	17 ± 7	28 ± 3	26 ± 2	351 ± 26	1.90 ± 0.15	157.3 ± 11.8	82.89 ± 8.94	a
	15-0210-068	L10-3-295	16 ± 9	11 ± 2	11 ± 9	16 ± 2	20 ± 2	299 ± 21	1.38 ± 0.10	227.4 ± 23	164.9 ± 20.68	a
	15-0210-069	L10-5-470	12 ± 4	9 ± 1	9 ± 4	16 ± 2	17 ± 1	253 ± 21	1.20 ± 0.09	148 ± 6.53	122.99 ± 10.61	a
A4	15-0210-071	L11-1-30	9 ± 8	11 ± 1	3 ± 9	26 ± 4	22 ± 2	279 ± 20	1.46 ± 0.11	143.3 ± 6.2	98.07 ± 8.45	a
	15-0210-072	L11-2-190	20 ± 8	11 ± 1	9 ± 6	19 ± 3	17 ± 1	295 ± 19	1.52 ± 0.11	227.2 ± 25.8	149.6 ± 20.3	a
	15-0210-073	L11-2-230	6 ± 9	8 ± 2	9 ± 10	15 ± 3	18 ± 2	278 ± 23	1.42 ± 0.11	204.5 ± 17.2	143.90 ± 16.40	a
A5	15-0210-074	L12-1-140	15 ± 5	15 ± 2	11 ± 4	15 ± 2	16 ± 1	254 ± 18	1.35 ± 0.10	124.0 ± 4.07	91.64 ± 7.49	a
	15-0210-079	L12-5-585	10 ± 7	10 ± 1	9 ± 7	15 ± 2	16 ± 1	279 ± 23	1.28 ± 0.09	128.8 ± 8.7	100.3 ± 10.0	a
	15-0210-080	L12-6-770	6 ± 8	11 ± 2	12 ± 9	20 ± 3	21 ± 2	267 ± 21	1.21 ± 0.09	173 ± 17	143.11 ± 17.86	a
	15-0210-082	L12-7-985	15 ± 6	10 ± 2	12 ± 6	15 ± 2	16 ± 1	260 ± 23	1.28 ± 0.10	294 ± 11.03	230.01 ± 20.13	b
B1	15-0210-001	L1-1-56	21 ± 9	15 ± 2	10 ± 7	21 ± 4	20 ± 2	242 ± 18	1.36 ± 0.11	6.40 ± 0.35	4.700 ± 0.450	b
	15-0210-004	L1-6-805	17 ± 5	14 ± 2	12 ± 4	19 ± 2	20 ± 1	221 ± 19	1.26 ± 0.10	151.4 ± 7.4	120.35 ± 11.41	a
	15-0210-005	L1-10-1293	21 ± 7	16 ± 2	16 ± 6	25 ± 5	27 ± 2	240 ± 16	1.38 ± 0.12	153 ± 2.52	110.55 ± 9.46	a
	15-0210-013	L1-25-3325	11 ± 13	14 ± 3	14 ± 12	15 ± 3	20 ± 3	289 ± 25	1.36 ± 0.12	234 ± 15	172.39 ± 18.46	a
B2	15-0210-047	L4-2-160	14 ± 5	14 ± 2	9 ± 4	17 ± 2	19 ± 1	289 ± 20	1.48 ± 0.11	86.06 ± 3.90	58.25 ± 5.07	a
	15-0210-048	L4-3-305	7 ± 6	10 ± 1	11 ± 8	12 ± 1	14 ± 1	241 ± 16	1.14 ± 0.08	66.64 ± 3.40	58.48 ± 5.15	a
	15-0210-049	L4-6-685	13 ± 4	12 ± 1	12 ± 4	17 ± 2	17 ± 1	301 ± 25	1.31 ± 0.10	77.91 ± 3.97	59.41 ± 5.33	a
	15-0210-051	L4-8-870	9 ± 6	7 ± 1	13 ± 7	10 ± 2	11 ± 1	178 ± 14	0.87 ± 0.07	62.71 ± 3.11	72.23 ± 6.57	a
	15-0210-053	L4-9-1055	13 ± 7	8 ± 1	1 ± 7	8 ± 2	10 ± 1	185 ± 14	0.92 ± 0.07	55.20 ± 3.13	59.945 ± 5.79	a
B3	15-0210-015	L2-1-110	14 ± 4	12 ± 2	10 ± 3	16 ± 2	17 ± 2	428 ± 25	1.80 ± 0.12	1.08 ± 0.09	0.600 ± 0.065	a
	15-0210-020	L2-3-260	15 ± 6	14 ± 2	14 ± 5	13 ± 2	16 ± 2	334 ± 23	1.63 ± 0.12	2.23 ± 0.07	1.37 ± 0.11	b
	15-0210-031	L2-9-905	13 ± 6	15 ± 2	11 ± 5	21 ± 3	19 ± 1	286 ± 19	1.32 ± 0.10	3.10 ± 0.11	2.35 ± 0.20	a
	15-0210-032	L2-11-1285	36 ± 15	19 ± 3	16 ± 12	23 ± 3	27 ± 3	356 ± 28	1.75 ± 0.15	3.65 ± 0.20	2.09 ± 0.210	a
	15-0210-036	L2-17-2115	19 ± 7	14 ± 2	11 ± 8	15 ± 2	16 ± 2	294 ± 20	1.14 ± 0.09	11.38 ± 0.82	9.98 ± 1.05	a
	15-0210-040	L2-17-2235	3 ± 17	7 ± 3	2 ± 16	11 ± 5	14 ± 3	223 ± 33	0.91 ± 0.09	11.91 ± 0.51	13.11 ± 1.42	a
B4	15-0210-041	L3-1-110	17 ± 8	11 ± 2	5 ± 5	19 ± 3	17 ± 2	274 ± 20	1.38 ± 0.10	111 ± 5.38	80.45 ± 7.19	a
	15-0210-043	L3-2-220	10 ± 11	16 ± 2	18 ± 9	23 ± 3	23 ± 2	356 ± 24	1.62 ± 0.12	153.8 ± 3.04	94.25 ± 7.22	a
	15-0210-045	L3-5-610	12 ± 4	10 ± 1	7 ± 3	16 ± 2	15 ± 2	204 ± 15	1.06 ± 0.08	165 ± 15.2	156.03 ± 18.03	a

† The age models are the following: a = central age model (CAM); b = minimum age model (MAM).

Using high-resolution gamma spectrometry, the quantities of lithogenic radionuclides, including  $^{238}\text{U}$ ,  $^{226}\text{Ra}$ ,  $^{210}\text{Pb}$ ,  $^{232}\text{Th}$ , and  $^{40}\text{K}$ , were examined in sediments next to OSL samples [28]. The calculation of dose rates was performed using the conversion factors [29] and  $\beta$ -attenuation factors [30]. The cosmic dosage rates were derived from [31], with an alpha-efficiency “ $\alpha$ ” value of  $0.04 \pm 0.02$  [32]. The water content of each sample was directly measured and considered to accurately represent the saturation levels throughout the whole burial period. To accommodate for any ambiguity, an error margin of  $\pm 5\%$  was applied.

#### Visualisation of OSL Ages

The utilisation of an adaptive kernel density estimation (AKDE) technique allows for a statistically reliable approach to visually represent the temporal distribution of optically stimulated luminescence (OSL) ages [33]. AKDE employs different bandwidths, utilising broader bandwidths in areas with limited data and narrower bandwidths in regions with abundant observations. The algorithm employed is the adaptive algorithm from reference [34], as explained by [35]. The initial bandwidth was determined using least squares cross-validation, commonly known as unbiased cross-validation [36]. Further elaboration on KDE and the process of selecting the bandwidth can be found in reference [37].

#### 2.2. Radiocarbon Dating

Beta Analytic laboratory conducted radiocarbon dating using established protocols [38]. The conventional age was determined based on the findings of reference [39]. The process of aligning with calendar years was conducted using the SHCAL13 database [40]. The radiocarbon ages are provided in calibrated years before present (cal a BP) in Table 2 and are converted to kilo-annum (ka) solely for the sake of presentation.

**Table 2.** Radiocarbon sample information and age estimates.

Core	Lab ID	Field ID	Material	d13C	Conventional RC Age (BP)	* RCYBP $2\sigma$
B3	L2-4-365	417310	Charred	−18.4 o/oo	$1500 \pm 30$	1365–1310
	L2-17-2115	417312	wood	−25.6 o/oo	$12530 \pm 40$	14820–14650
	L2-17-2195	417311	wood	−26.7 o/oo	$12570 \pm 40$	14960–14730

\* Calibrated radiocarbon age (BP = 1950 AD).

#### 2.3. Aggradation Rates

Aggradation rates (AR) were calculated for each unit based on the OSL age and its depth below the surface as

$$AR = \frac{(D_i - D_{i-1})}{(T_i - T_{i-1})}$$

where  $D_i$  and  $T_i$  are the depth and age of the OSL-sample, respectively, and  $T_{i-1}$  and  $D_{i-1}$  are the age and depth of the following stratigraphic younger OSL sample.  $T_i$  represents the mean value of the  $1\sigma$ -age range. A mean aggradation rate was calculated for each site with  $\geq 2$  samples.

### 3. Results

The bedrock palaeovalley is evident in the DEM downstream of Gatton where the Lockyer Creek is laterally confined by bedrock in several locations (Figure 2). The depth to bedrock reaches a maximum upstream of the confluence with the mid-Brisbane River (Figure 2). The reconstructed bedrock profile shows subtle vertical height differences at several locations, which appear unrelated to changes in catchment area and tributary inputs (Figure 3). Given the uncertainty in extracting depth estimates, and the fact that these are now buried, their interpretation as knickpoints remains unsupported. However, in the upper reaches of the Lockyer Creek two knick-points are clearly visible in the present channel bed at  $\sim 110$  km and 120 km upstream (Figure 3).

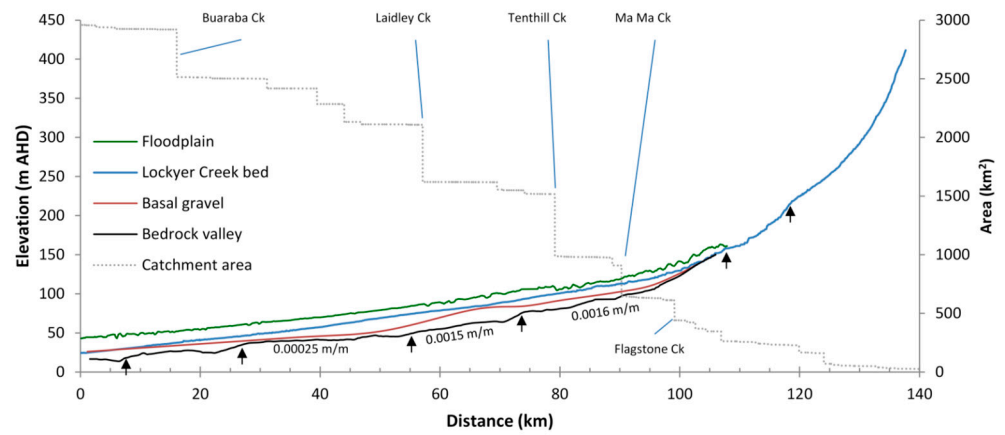


**Figure 3.** Long profile of the bedrock valley, gravel, and fine-grained floodplain units, together with the current thalweg of the Lockyer. The dotted line portrays the stepwise increases in drainage area for the Lockyer Creek as it is joined by tributaries. Floodplain surface measured proximal to the main channel.

A relatively continuous coarse gravel unit overlies bedrock and is mapped longitudinally and laterally from the confluence upstream to the town of Helidon (Figure 3). The floodplain fines show a thickening downstream, but there is no obvious association with tributary inputs and increases in catchment-contributing area (Figure 3).

### 3.1. Valley Fill Chronostratigraphy

At cross-section A, the current Lockyer Creek sits on the northern valley margin in a single bedrock valley (Figure 4). At cross-section B, the current Lockyer Creek sits centrally within a narrow bedrock valley (~200 m wide), one of three at this cross-section (Figure 5). Four cores were extracted to an average depth of 28 m across the 2.5 km valley floor (Figure 5). Table 1 provides a detailed summary of the OSL chronological dataset. The radiocarbon chronological dataset is provided in Table 2.

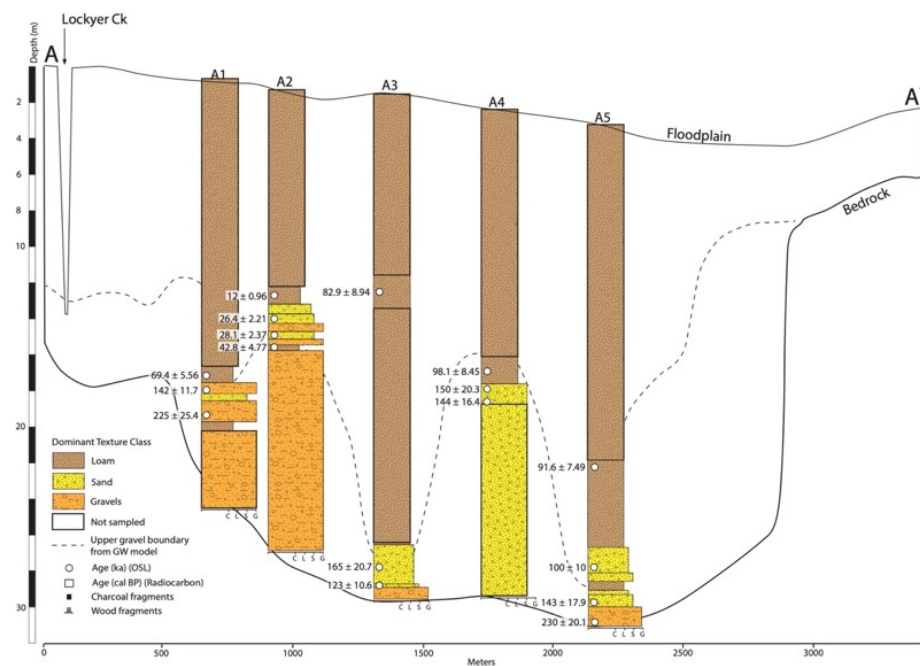


**Figure 4.** Chronostratigraphic units at cross-section A. The black outline shows core depths not sampled in this study. A1–A5 denote the location of the selected drilling locations.

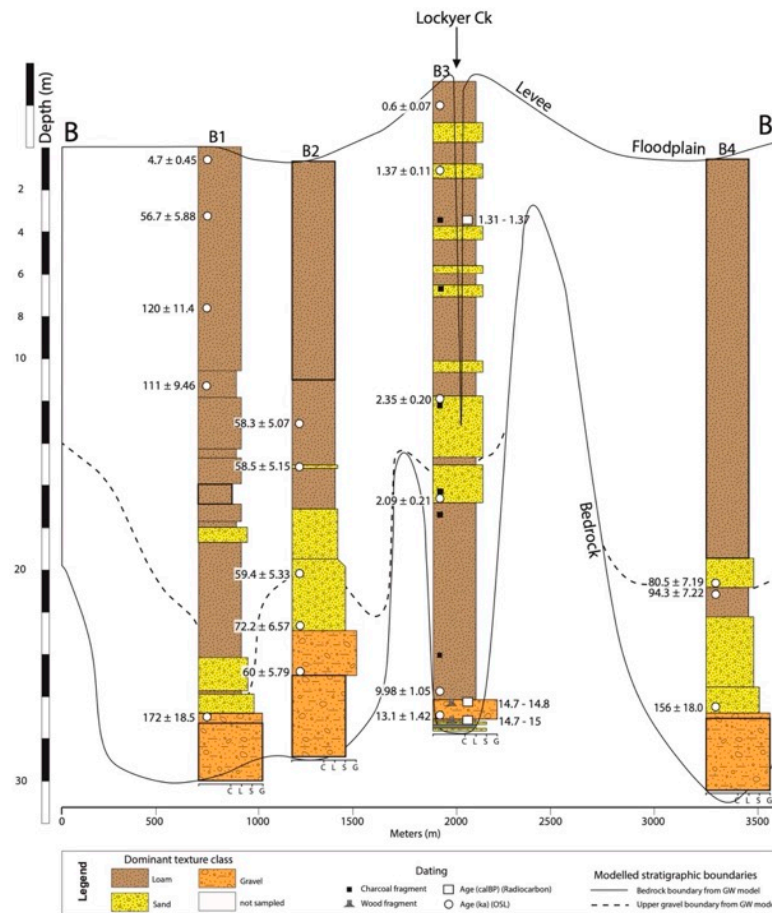


**Figure 5.** Chronostratigraphic units at cross-section B. The black outline shows core depths not sampled in this study. B1–B4 refer to the locations of drill sites at this cross-section.

### 3.1.1. Coarse Channel Deposits

Basal channel deposits in Core A1 were sampled at ~18 m, confirming the estimated depth in the groundwater database. The upper contact of this unit consisted of well-sorted gravels and small pebbles (~5 cm in diameter) which produced a date of  $225 \pm 25$  ka (Figure 4). This was overlain by a thin unit of coarse sands dated to  $142 \pm 12$  ka. The contact between the gravel and the coarse sands was sharp, with no evidence of preserved bedding or a fining upward sequence. Similar calibre units are located at 29 m in Core A5 and dated to  $144 \pm 16$  and  $230 \pm 20$  ka, respectively. These are coeval with the channel units dated in Core A1 (Figure 4). The two samples taken within 0.5 m of each other in Core A4 produced very similar ages ( $144 \pm 16$  and  $150 \pm 20$ ) and provide confidence in the age of this unit. At Core A3, a thin, coarse-sand layer was sampled from ~28 m in the profile and was dated to  $123 \pm 11$  ka. The age of these basal units is coeval with the coarse sands dated at ~145 ka in laterally adjacent cores. The height of the upper boundary of this unit varies significantly (with ~18 m in Cores A1 and A4 and ~10 m lower in Cores A3 and A5), indicating significant localized post-depositional incision.

In Core A2, coarse units between 13 and 15.5 m were dated to  $28 \pm 2.4$  ka and  $26 \pm 2$  ka (Figure 4). A silty clay located beneath the coarse units (~15 m) was dated to  $43 \pm 5$  ka and indicates a significant hiatus (>20 ka) between these units.

Basal sands in Core B1 were dated to  $172 \pm 18$  ka, which is within error of the date of  $156 \pm 18$  ka in an equivalent unit in Core B4 at ~27 m depth. This core is located in the bedrock valley on the southern valley margin and is separated from the adjacent cores (B1–B3) by a pronounced bedrock spur (located at 1700 and 2500 m on the cross-section Figure 5) (e.g., Figure 2 transect B). A thinner unit of coarse fluvial sands was sampled at

~20 m depth in this core, which yielded an age of  $80 \pm 7$  ka. It was found directly overlying a thin, fine-grained unit of silty loam (Figure 5).

Basal units of sands and gravels in Core B2, located between 17 and 25 m depth, produced ages ranging from  $60 \pm 6$  ka to  $72 \pm 6$  ka, with all ages within error.

Core B3 is located within the levee of the present Lockyer creek, which stands ~4 m above the distal floodplain (Figure 5). A basal unit of channel sands and gravels located between 29–31 m was dated at  $13 \pm 1$  ka (Figure 5). Within this unit, thin layers of organic-rich, mud-dominated deposits were identified, in which wood fragments were found and dated to 14.7–15 cal a BP (Beta—417311) and 14.7–14.8 cal a BP (Beta—417312) (Table 2). A coarse-grained unit is also located at 12 to 17 m depth, equivalent to the bed of the current channel, and returned within error dates between  $2.09 \pm 0.21$  and  $2.35 \pm 0.2$  (Figure 5).

The AKDE plot (Figure S5) was used to determine and visualise the grouping of the coarse deposits ( $n = 22$ ) age data, highlighting distinct ‘peaks’ at ~223, 144, 62, 27, 14, and 2 ka.

### 3.1.2. Fine-Grained Units

Two overbank units are differentiated based on grain size and sedimentology: (1) sand units containing high percentages of silts and clays are interpreted as crevasse splay deposits; and (2) fine-grained silts and clays that have no internal structure or preserved bedding and, except for Core B3, show no vertical changes in particle size down the profile (Figure S3). These are considered representative of deposition within shallow subaqueous environments such as flood basins and floodplain swamps, which persist today on the modern floodplain surface.

In cross-section A, the oldest fine-grained unit was sampled from ~14 to 21 m in the profile was dated to  $98 \pm 8$  ka and  $92 \pm 7$  ka in Cores A4 and A5, respectively (Figure 4). Older dates of  $110 \pm 9$  ka and  $120 \pm 11$  ka were returned for the fine-grained silts and clays present in Core B1 at between 12–8 m in the profile (Figure 5). A later period of fine-grained deposition is recorded in Core B2, where samples at 15 m and 13 m were dated to  $58 \pm 5.15$  and  $58 \pm 5.07$  ka. A chronologically equivalent unit was found at 2 m in Core B1 and dated to  $57 \pm 6$  ka, which is within error of the B2 samples (Figure 5). The upper unit in Core B1 is dated to  $4.7 \pm 0.45$  ka, confirming deposition in the distal margin of the floodplain at this site.

The alternating units of fine-grained silty loams and coarser-grained sands in core B3 (Figure S3) are dated to  $1.37 \pm 0.11$  ka and  $1.35 \pm 0.05$  ka from OSL and radiocarbon dating, respectively. These are interpreted as crevasse splay deposits and the near surface (c. 1 m) age of  $0.6 \pm 0.07$  ka confirms ongoing deposition within the current levee system.

### 3.1.3. Aggradation Rates

Aggradation rates were constructed at cross-section B, where units were better constrained chronologically (Figure 6). These show significant differences in fine-grained aggradation, with Core B1 showing low sedimentation rates ( $0.08 \text{ m ka}^{-1}$ ) over the last c. 120 ka compared to Core B2 ( $0.24 \text{ m ka}^{-1}$ ). The most compelling contrast occurs in comparison with the sedimentation rates in Core B3 ( $2.57 \text{ m ka}^{-1}$ ) within the current levee-dominated channel system, which are between 3 and 11 times higher (Figure 6).

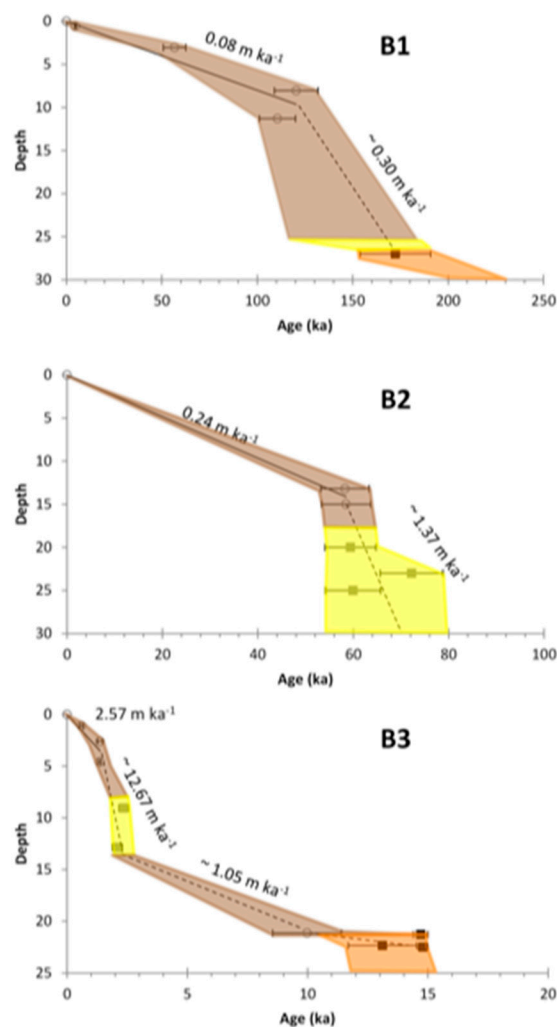


**Figure 6.** Aggradation rates ( $\text{m ka}^{-1}$ ) for Cores B1, B2, and B3. Dashed lines and ~symbol used to indicate aggradation rates of greater uncertainty between different units. Orange = gravels; yellow = sands; brown = loam.

#### 4. Discussion

The 30 m of aggradation recorded here spans the last 220 ka and is the result of extensive alluvial sediment phases that have infilled the alluvial valley of the Lockyer Creek. Before delving into the importance of these findings, it is necessary to address the uncertainty surrounding the data. The groundwater bore logs, which demonstrated a high level of accuracy within a 1 m range from our drilling, allowed us to analyse and understand the alluvial sequences in relation to the bedrock morphology of the valley. Intermittent occurrences of exposed bedrock or shallow elevated areas within the alluvium have been observed to significantly impact the movement and containment of rivers, as well as the thickness of sediment deposits [20]. Extracting the bedrock digital elevation model (DEM) was challenging due to the difficulty in precisely determining the depths to and within the bedrock along the whole length of the main Lockyer channel. The technique used to determine the depth and vertical consistency of the coarse-gravel layer in the valley-fill sequence is prone to some degree of inaccuracy, and it is incapable of capturing more nuanced variations in bed elevation, which may manifest as ‘apparent knickpoints’. However, there is undeniable evidence of a greatly fluctuating bedrock valley shape characterised by alternating elevated and depressed areas, within which the current Lockyer River has eroded.

Although the chosen cross-sections in this work accurately depicted the overall structure of alluvial sequences, the use of bore log data to identify specific chronostratigraphic units has certain limits, as validated by independent dating. For instance, the base gravel unit that appeared as a single unit in the bore-log data was actually found to consist of two distinct units, which were divided by thin sedimentological changes that were not well defined. Similarly, while the fine-grained members may seem continuous, dating evidence reveals that they actually differ in age. In certain instances, the age difference might exceed 50 thousand years in boreholes that are less than 500 metres apart. The application of chronological controls in this study allows for the accurate representation of the intricate nature of this complexity. It also emphasises the potential occurrence of inaccuracies in interpreting late Quaternary fluvial records in lowland areas lacking sufficient exposure. This is particularly applicable to coastal rivers in eastern Australia, where there is a lack of distinct topographic terraces resulting in neighbouring sequences known as polycyclic terraces [41].

The sample size for OSL dating in this study ( $n = 36$ ) is similar to that employed in bigger basins [42,43]. Additionally, sampling within the same stratigraphic level and utilising C14 radiocarbon dating further enhances confidence. Nevertheless, it is probable that the older samples include a substantial amount of grains that would produce a signal that is near or above saturation. Thomsen et al. (2016) [44] examined the potential influence of saturation on the ultimate age determination and suggested techniques to mitigate this influence. However, these techniques were not implemented in the present work. Similarly, although attempts were made to address feldspar contamination using the SAR method, these measures are expected to simply reduce, rather than eliminate, feldspar contamination.

#### 4.1. Phases of Incision and Aggradation

The fluvial sedimentary record presented here for the last c. 220 ka is one of the oldest documented for Australia and allows us to reconstruct the sequence of major cut and fill episodes for this sub-tropical basin (Figure 7). The first channel aggradation phase is represented by the basal gravel unit, which has a pooled mean age of ~220 ka (marine isotope sub-stage 7d) (Figure 7a). Little is known about precipitation and associated river discharge characteristics during this time, except for Cooper Creek in central Australia, which was reported to have had mean bankfull discharges 5–7 times larger than today 230–250 ka years ago [45]. In the Lockyer record, this period is characterised by coarse bedload, which implies sufficiently high discharges for bedload transport across wide valley floors. This unit is also preserved as a basal lag in the terrace sequences in the upper reaches at Helidon [46], suggesting a valley-wide depositional response to laterally mobile channels. A unit of coarse basal gravels sampled at depth (~18 m) in the valley fill of the Comet River in the Fitzroy River Basin also shows evidence of coarse-grained fluvial activity at ~196 ka [42].

Considerable focus has been placed on the climate patterns of MIS 5 and the characteristics of related weather changes in central Australia [47,48]. The most probable reason for periods of increased river activity and lake filling during MIS 5e is believed to be the higher amount of rainfall [45,47]. This period is also linked to past high river flows, which were 5–8 times larger than current levels on the Riverine Plain [7,9]. There are not many records of rivers during this time in the subtropical region, but there is some evidence of increased river activity during MIS 5 in the Fitzroy Basin [42]. However, it is recognised that the lack of a clear climate signal may be due to the limited preservation of sediment in older units in large basins [42]. Although we cannot ignore this influence in the Lockyer record, this period is marked by mostly fine-grained overbank deposition and reasonably consistent aggradation.

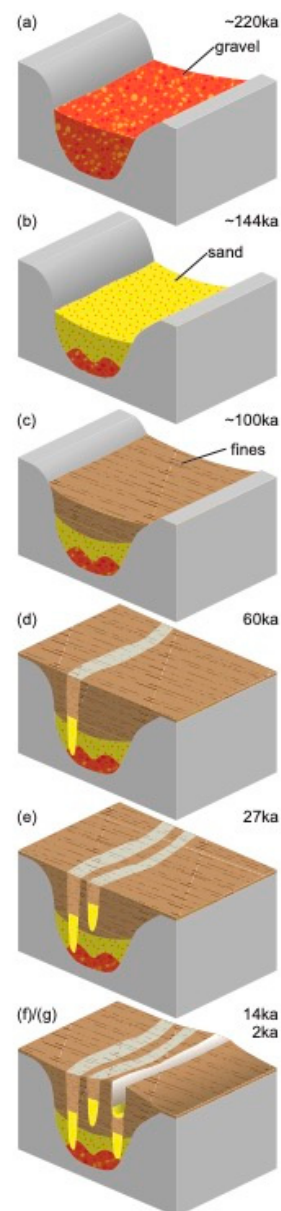


**Figure 7.** A schematic outlining the major phases of channel aggradation identified in the valley fill record of the lower Lockyer Creek.

On the other hand, the MIS 3 fluvial episode, which was previously observed in temperate Australia [4,7–9] and in the chronology of the Fitzroy Basin [42], is also identified in the Lockyer by the occurrence of incision and aggradation dating back to around 60,000 years ago. This was also apparent in the middle sections near Helidon, where the basal-lag deposits in the terrace sequence indicated an age of 56 ka [46]. In the central parts of the Lockyer Valley, this time period is connected to a significant stage of terrace formation. These terraces are made up of large gravels covered by fine silts and clay which have been dated to be between  $34.8 \pm 3.6$  thousand years ago and  $10.3 \pm 1.4$  thousand years ago [46]. Together, this indicates that there is a basin-wide response to increased discharges.

A second-to-last phase of channel incision before approximately 14 thousand years ago saw the lower Lockyer River move to its present location on the valley floor (e.g., B3 in Figure 5). The incision into bedrock during this stage reached a depth of 30 m (Figure 5). The climatic conditions during the Last Glacial Maximum (MIS 2) in Australia were previously believed to be among the driest ever recorded. However, recent research indicates that the circumstances may have been significantly wetter [48] and/or more unpredictable [48–50].

A recent study conducted in sub-tropical coastal Australia, located just a few kilometres away from the Lockyer Creek basin, suggests that the Last Glacial Maximum (LGM) had two distinct periods of dryness, with a wetter climate in between [51]. The Lockyer Creek has signs of less river activity at this period, indicating a potentially less humid climate during the Last Glacial Maximum (LGM). On the other hand, data from the Fitzroy Basin showed a period of increased rainfall, which is seen in the higher river activity in the Nogoia sub-catchment [42]. It seems that the level of detail needed to determine if rivers respond synchronously to wet/dry conditions during the Last Glacial Maximum (LGM) is not currently accessible. Further research is necessary in the entire region to completely address this matter.

During the last glacial period, the chronologies of sediment deposits in the Lake Eyre Basin and south-eastern Australia indicate a shift towards more wetter conditions (summarised in [5]). This coincides with the time when terraces were abandoned in the upper Lockyer, around 10,000 years ago [46], and when the lower Lockyer started to erode, around 13,000 years ago. Additional data suggest a decrease in rainfall around 6000 years ago [52] and an increase in climate variability starting around 4500 years ago due to the strengthening of ENSO activity and the establishment of the current climate [53–56]. The consistently detailed nature of the vertical accretion deposits during this time makes understanding any climatic influence difficult, beyond the broader interpretation that vegetation and discharge conditions provided enough material and space for deep sequences of valley accumulation. Nevertheless, the presence of clearly distinguishable alternating fine- and coarse-grained units around 2 ka is significant and is believed to indicate flood conditions with increased intensity, which are probably linked to an intensification of ENSO activity. The rate of sediment accumulation for this Holocene unit is approximately 11 times higher than the rate estimated from surrounding cores over a longer period of time. This comes after a presumed decrease in rainfall around 6000 years ago [6,51] and the start of more variable climate around 4500 years ago when ENSO activity began, and the current climate was established [54].

#### 4.2. Base-Level Adjustments

It would appear from the chronostratigraphic record that climate variability alone cannot fully explain the nature and timing of fluvial response in the lower Lockyer. Other key controls are likely to be base-level adjustments, both at tributary junctions and downstream at the confluence with the mid-Brisbane. However, determining the upstream influence of eustatic or local base-level adjustments over this timescale is not straightforward. Several factors act to inhibit fluvial incision during base-level fall, including the time available for fluvial systems to adjust to base-level shifts and the resistance of the underlying strata [57]. The error bars on the MIS 7 and 6 OSL ages preclude too much inference on the timing of fluvial response to any base-level adjustment during these stages. While the older gravel deposits (dated to ~220 and 145 ka and 60 ka) broadly align with the low sea-level stands, later channel incisional phases dated to between 27–12 ka pre- and post-date the last glacial low stand (corresponding to the –130 m isobath) [58] (Figure 8). Importantly, terrace incisional phases described in the upper reaches of the valley at ~10 ka occurred as the sea level rapidly rose from –30 m below present mean sea level to +0.5–1.5 m above modern at ~7 cal. ka BP [58]. Daley and Cohen (2018) [59], for example, discount the impacts of an immediate sea level response in their interpretation of the timing of terrace abandonment in the upper Lockyer and several adjacent catchments. Local base-level adjustments in the Lockyer-Brisbane confluence zone may have played an important role in floodplain sedimentation style and aggradation rates in the lower reaches. A lidar image of the confluence shows a complex floodplain morphology relative to upstream reaches, with flood chutes and backwater channels (Figure 9). As evident during the extreme floods in 2011 and 2013, extensive backwater inundation in this zone occurs due to the coincident timing of flood discharges down the Lockyer and mid-Brisbane rivers [60]. A series of well-preserved paleochannels in this reach also suggests that the Lockyer Creek may have

exited and joined the mid-Brisbane elsewhere at some early stages of valley and channel evolution (Figure 9), and changes in channel gradient and length would have had a marked effect on floodplain sedimentation patterns and rates. Reconstructing the record of flooding in this valley over the past millennia shows at least six stages of extreme flooding over the past 2000 years, which are likely to have induced this type of backwater inundation at the confluence [61]. Notably, an event approximately 300 years ago (1730 AD) is believed to have stripped valley alluvium and reset the channel to bedrock [61].

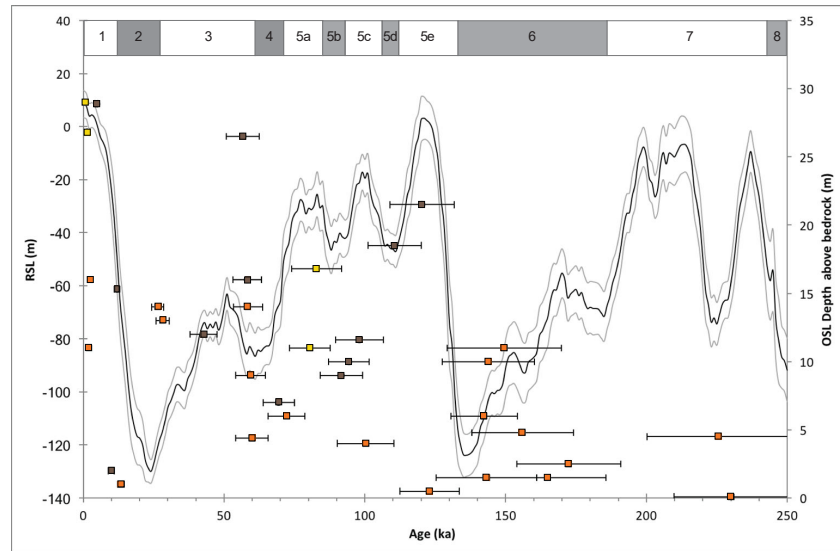


**Figure 8.** The distribution of OSL ages with 2 sigma error for both coarse gravels (orange square), coarse sands (yellow square) and fine-grained silty/loam deposits (brown/grey square) against relative sea level (solid black curve) and depth to bedrock. Relative sea level compiled from Spratt and Lisiecki (2016) [56], with solid grey lines denoting the 1 sigma error envelope.

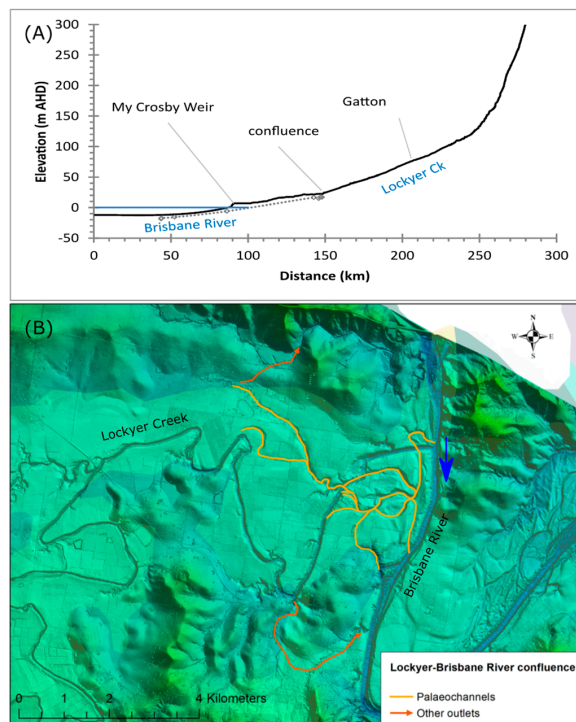


**Figure 9.** (A) Long profile of the mid-Brisbane River from Moreton Bay to the confluence of the Lockyer Creek. The dashed grey line is the interpolated bedrock profile with known sites of bedrock

exposure. (B) Lidar image of the confluence of the Lockyer with the mid-Brisbane showing the distribution of paleochannels and possible alternative tributary junctions.

## 5. Conclusions

This study gives one of the first reconstructions of the timing and characteristics of river response over previous glacial/interglacial cycles in sub-tropical Australia. Several points are of note; firstly, the majority of the sediment in the lower Lockyer Valley is made up of fine-grained alluvial deposits. Secondly, valley floor aggradation during Marine Isotope Stages 7, 6, and 5, and the incision during Marine Isotope Stage 3, seem to have occurred without being influenced by significant variations in sea level. Nevertheless, local changes around the main junction of the tributary with the Brisbane River, along with an uneven bedrock surface, probably had a significant influence on the primary pattern of fine-grained vertical sediment accumulation. During the last 2 thousand years, there has been a noticeable change in the rate and way in which sediment accumulates, due to the formation of crevasse splays and levees which is probably linked to the more frequent and intense floods caused by ENSO events.

On a larger scale, beyond having been a case study in the geologically stable settings of eastern Australia, some of the findings mentioned here might be applicable to future studies. This study had access to a wide range of historical and sedimentological data, and the Lockyer Valley is a highly researched area in Australia because of a major flood event that took place there in 2011 [17]. However, it was still difficult to untangle the influence of important factors on the process of river aggradation and incision. The fine-grained, vertical accretion deposits in the floodplains are frequently inadequate records of previous climatic alterations. The related large channels, which experience frequent periods of expansion and contraction caused by extreme events [60], also provide difficulties in identifying any related changes in climate-induced discharges. However, the significant scale of channel incision that occurred during the most recent period of river adjustment after 3 ka is important as the basin is not affected by tectonic activity. This shows how episodic catastrophic flood episodes can have a significant impact on the preserved sedimentary signals and patterns even in small basins.

**Supplementary Materials:** The following supporting information can be downloaded at: <https://www.mdpi.com/article/10.3390/quat7010009/s1>. Figure S1. OSL dating methodology included preheat plateau testing done on a range of samples that represented the population from the region, with preheat and cut heat set at 240- and 180-degrees centigrade. A standard 10 s dose irradiation was applied to each run, and the dose response recovery was measured. Figure S2 illustrates outputs used to identify saturated grains using test dose response curves. In the first example, the quartz grain had an accumulated signal considerably higher than the top standard (3500 s) irradiation used for this sample. Note that the test dose response was within  $\pm 20\%$ . This grain was rejected from the calculation. In the second example, the quartz grain had accumulated a signal in the field that was considerably higher than what could be artificially applied and was determined to be saturated. This sample was not included in the analysis. Figure S3 displays down-core particle size distributions for (A) Core B1 and (B) Core B3, showing percentages of gravel, sand, silt, and clay. Figure S4 shows Quartz OSL radial plots and graphical representations of  $PDF_{\text{Gaussian}}$  distributions for older samples: (A) sample 15-0210-0013 with an overdispersion of  $\sim 12\%$ , CAM accepted, and multiple peaks are within uncertainty of each other; (B) sample 15-0210-0068 with an overdispersion of  $\sim 21\%$ . CAM, MAM and FMM (2 component mix) all identified multiple peaks within uncertainty of each other; the CAM was accepted. Figure S5 displays an adaptive kernel density estimate (AKDE) showing major modes in the distribution of the OSL ages of the coarse bedload samples.

**Author Contributions:** Conceptualization, J.C. and C.T.; methodology, J.C., C.T. and A.L.; formal analysis, J.C. and A.L.; writing—original draft preparation, J.C., A.L., C.T., K.H. and M.M.; writing—review and editing, J.C., A.L., K.H. and M.M.; visualization, C.T., A.L. and K.H.; funding acquisition, J.C. and M.M. All authors have read and agreed to the published version of the manuscript.

**Funding:** This research was funded by the Australian Research Council Linkage Award (LP120200093).

**Data Availability Statement:** The data presented in this study are available on request from the corresponding author (jacky.croke@qut.edu.au).

**Acknowledgments:** We thank members of the Landscape Science team Department of Environment and Science (DES) for their expertise in drilling and Bernie Powell, who provided advice and expertise on the soils of the Lockyer Valley. We thank Ashneel Sharma (DES) for conducting the OSL analyses reported in this study and Tim Pietsch (Griffith University) for assistance in interpreting the data.

**Conflicts of Interest:** The authors declare no conflicts of interest. The funders had no role in the design of the study; in the collection, analyses, or interpretation of data; in the writing of the manuscript; or in the decision to publish the results.

## References

1. Westaway, R.; Bridgland, D.R.; Sinha, R.; Demir, T. Fluvial sequences as evidence for landscape and climatic evolution in the Late Cenozoic: A synthesis of data from IGCP 518. *Glob. Planet. Chang.* **2009**, *68*, 237–253. [\[CrossRef\]](#)
2. Bridgland, D.R.; Keen, D.H.; Westaway, R. Global correlation of late Cenozoic fluvial deposits: A synthesis of data from IGCP 449. *Quat. Sci. Rev.* **2007**, *26*, 2694–2700. [\[CrossRef\]](#)
3. Macklin, M.G.; Lewin, J.; Woodward, J.C. The fluvial record of climate change. *Philos. Trans. R. Soc. Lond. A* **2012**, *370*, 2143–2172. [\[CrossRef\]](#) [\[PubMed\]](#)
4. Nanson, G.; Cohen, T.J.; Doyle, C.J.; Price, D.M. Alluvial evidence of major late Quaternary climate and flow regime changes on the coastal rivers of New South Wales, Australia. In *Palaeohydrology: Understanding Global Change*; Gregory, K.J., Benito, G., Eds.; Wiley & Sons: Hoboken, NJ, USA, 2003; pp. 233–258.
5. Nanson, G.C.; Price, D.M.; Short, S.A. Wetting and drying of Australia over the past 300 ka. *Geology* **1992**, *20*, 791–794. [\[CrossRef\]](#)
6. Petherick, L.; Bostock, H.; Cohen, T.J.; Fitzsimmons, K.; Tibby, J.; Fletcher, M.S.; Moss, P.; Reeves, J.; Mooney, S.; Barrows, T.; et al. Climatic records over the past 30 ka from temperate Australia—A synthesis from the Oz-INTIMATE workgroup. *Quat. Sci. Rev.* **2013**, *74*, 58–77. [\[CrossRef\]](#)
7. Kemp, J.; Rhodes, E.J. Episodic fluvial activity of inland rivers in southeastern Australia: Palaeochannel systems and terraces of the Lachlan River. *Quat. Sci. Rev.* **2010**, *29*, 732–752. [\[CrossRef\]](#)
8. Kemp, J.; Spooner, N.A. Evidence for regionally wet conditions before the LGM in southeast Australia: OSL ages from a large palaeochannel in the Lachlan Valley. *J. Quat. Sci.* **2007**, *22*, 423–427. [\[CrossRef\]](#)
9. Page, K.; Nanson, G.; Price, D. Chronology of Murrumbidgee River palaeochannels on the Riverine Plain, southeastern Australia. *J. Quat. Sci.* **1996**, *11*, 311–326. [\[CrossRef\]](#)
10. Page, K.J.; Nanson, G.C.; Price, D.M. Thermoluminescence chronology of late quaternary deposition on the riverine plain of South-Eastern Australia. *Aust. Geogr.* **1991**, *22*, 14–23. [\[CrossRef\]](#)
11. Hughes, K.; Croke, J. How did rivers in the wet tropics (NE Queensland, Australia) respond to climate changes over the past 30,000 years? *J. Quat. Sci.* **2017**, *32*, 744–759. [\[CrossRef\]](#)
12. Cheetham, M.D.; Bush, R.T.; Keene, A.F.; Erskine, W.D. Nonsynchronous, episodic incision: Evidence of threshold exceedance and complex response as controls of terrace formation. *Geomorphology* **2010**, *123*, 320–329. [\[CrossRef\]](#)
13. Cohen, T.J.; Nanson, G.C. Mind the gap: An absence of valley-fill deposits identifying the Holocene hypsithermal period of enhanced flow regime in southeastern Australia. *Holocene* **2007**, *17*, 411–418. [\[CrossRef\]](#)
14. Powell, B. *Nature, Distribution and Origin of Soils on an Alluvial Landscape in the Lockyer Valley, South-East Queensland*; University of New England: Portland, OR, USA, 1987.
15. Croke, J.; Todd, P.; Thompson, C.; Watson, F.; Denham, R.; Khanal, G. The use of multi temporal LiDAR to assess basin-scale erosion and deposition following the catastrophic January 2011 Lockyer flood, SE Queensland, Australia. *Geomorphology* **2013**, *184*, 111–126. [\[CrossRef\]](#)
16. Kiem, A.S.; Franks, S.W.; Kuczera, G. Multi-decadal variability of flood risk. *Geophys. Res. Lett.* **2003**, *30*, 36-1–36-4. [\[CrossRef\]](#)
17. Thompson, C.; Croke, J. The geomorphic effects, flood power and channel competence of a catastrophic flood in confined and unconfined reaches of the upper Lockyer valley, south east Queensland, Australia. *Geomorphology* **2013**, *197*, 156–169. [\[CrossRef\]](#)
18. Thompson, C.; Croke, J.; Dent, C. Potential Impacts of levee in construction in the Lockyer Valley. In Proceedings of the 7th Australian Stream Management Conference, Townsville, QLD, Australia, 27–30 July 2014; p. 7.
19. Apan, A.A.; Raine, S.R.; Paterson, M.S. Mapping and analysis of changes in the riparian landscape structure of the Lockyer Valley catchment, Queensland, Australia. *Landsc. Urban Plan.* **2002**, *59*, 43–57. [\[CrossRef\]](#)
20. Raiber, M.; Lewis, S.; Cendon, D.; Cui, T.; Cox, M.; Gilfedder, M.; Rassam, D. Significance of the connection between bedrock, alluvium and streams: A spatial and temporal hydrogeological and hydrogeochemical assessment from Queensland, Australia. *J. Hydrol.* **2019**, *569*, 666–684. [\[CrossRef\]](#)
21. Folk, R.L. The Distinction between Grain Size and Mineral Composition in Sedimentary-Rock Nomenclature. *J. Geol.* **1954**, *62*, 344–359. [\[CrossRef\]](#)
22. Olley, J.M.; Pietsch, T.; Roberts, R.G. Optical dating of Holocene sediments from a variety of geomorphic settings using single grains of quartz. *Geomorphology* **2004**, *60*, 337–358. [\[CrossRef\]](#)

23. Pietsch, T.J. Optically stimulated luminescence dating of young (<500 years old) sediments: Testing estimates of burial dose. *Quat. Geochronol.* **2009**, *4*, 406–422. [[CrossRef](#)]
24. Galbraith, R.F.; Laslett, G.M. Statistical models for mixed fission track ages. *Nucl. Tracks Radiat. Meas.* **1993**, *21*, 459–470. [[CrossRef](#)]
25. Galbraith, R.F.; Roberts, R.G.; Laslett, G.M.; Yoshida, H.; Olley, J.M. Optical Dating Of Single And Multiple Grains Of Quartz From Jinmium Rock Shelter, Northern Australia: Part I, Experimental Design And Statistical Models. *Archaeometry* **1999**, *41*, 339–364. [[CrossRef](#)]
26. Roberts, H.M.; Wintle, A.G. Equivalent dose determinations for polymineralic fine-grains using the SAR protocol: Application to a Holocene sequence of the Chinese Loess Plateau. *Quat. Sci. Rev.* **2001**, *20*, 859–863. [[CrossRef](#)]
27. Arnold, L.J.; Roberts, R.G.; Galbraith, R.F.; DeLong, S.B. A revised burial dose estimation procedure for optical dating of young and modern-age sediments. *Quat. Geochronol.* **2009**, *4*, 306–325. [[CrossRef](#)]
28. Murray, A.S.; Marten, R.; Johnston, A.; Martin, P. Analysis for naturally occurring radionuclides at environmental concentrations by gamma spectrometry. *J. Radioanal. Nucl. Chem.* **1987**, *115*, 263. [[CrossRef](#)]
29. Stokes, S.; Hetzel, R.; Bailey, R.M.; Mingxin, T. Combined IRSL-OSL single aliquot regeneration (SAR) equivalent dose (De) estimates from source proximal Chinese loess. *Quat. Sci. Rev.* **2003**, *22*, 975–983. [[CrossRef](#)]
30. Guérin, G.; Mercier, N.; Nathan, R.; Adamiec, G.; Lefrais, Y. On the use of the infinite matrix assumption and associated concepts: A critical review. *Radiat. Meas.* **2012**, *47*, 778–785. [[CrossRef](#)]
31. Prescott, J.R.; Hutton, J.T. 1994 Cosmic ray contributions to dose rates for luminescence and ESR dating: Large depths and long-term time variations. *Radiat. Meas.* **1994**, *23*, 497–500. [[CrossRef](#)]
32. Bowler, J.M.; Johnston, H.; Olley, J.M.; Prescott, J.R.; Roberts, R.G.; Shawcross, W.; Spooner, N.A. New ages for human occupation and climatic change at Lake Mungo, Australia. *Nature* **2003**, *421*, 837–840. [[CrossRef](#)]
33. Vermeesch, P. On the visualisation of detrital age distributions. *Chem. Geol.* **2012**, *312–313*, 190–194. [[CrossRef](#)]
34. Abramson, I.S. On Bandwidth Variation in Kernel Estimates-A Square Root Law. *Ann. Stat.* **1982**, *10*, 1217–1223. [[CrossRef](#)]
35. Jann, B. *Univariate Kernel Density Estimation*; Statistical Software Component S456410; College Department of Economics: Chestnut Hill, MA, USA, 2007. Available online: <http://fmwww.bc.edu/RePEc/bocode/k/kdens.pdf> (accessed on 2 January 2024).
36. Hall, P. Large Sample Optimality of Least Squares Cross-Validation in Density Estimation. *Ann. Stat.* **1983**, *11*, 1156–1174. [[CrossRef](#)]
37. Sheather, S.J. Density Estimation. *Stat. Sci.* **2004**, *19*, 588–597. [[CrossRef](#)]
38. Beta Analytic Inc. *Introduction to Radiocarbon Determination by the Accelerator Mass Spectrometry Method*; Beta Analytic Inc.: Miami, FL, USA, 2015.
39. Talma, A.S.; Vogel, J.C. A simplified approach to calibrating <sup>14</sup>C dates. *Radiocarbon* **1993**, *35*, 317–322. [[CrossRef](#)]
40. Hogg, A.G.; Hua, Q.; Blackwell, P.G.; Niu, M.; Buck, C.E.; Guilderson, T.P.; Heaton, T.J.; Palmer, J.G.; Reimer, P.J.; Reimer, R.W.; et al. SHCal13 Southern Hemisphere Calibration, 0–50,000 Years cal BP. *Radiocarbon* **2013**, *55*, 1889–1903. [[CrossRef](#)]
41. Cohen, T.J.; Nanson, G.C. Topographically associated but chronologically disjunct late Quaternary floodplains and terraces in a partly confined valley, south-eastern Australia. *Earth Surf. Process. Landf.* **2008**, *33*, 424–443. [[CrossRef](#)]
42. Croke, J.; Jansen, J.D.; Amos, K.; Pietsch, T.J. A 100 ka record of fluvial activity in the Fitzroy River Basin, tropical northeastern Australia. *Quat. Sci. Rev.* **2011**, *30*, 1681–1695. [[CrossRef](#)]
43. Pietsch, T.J.; Nanson, G.C.; Olley, J.M. Late Quaternary changes in flow-regime on the Gwydir distributive fluvial system, southeastern Australia. *Quat. Sci. Rev.* **2013**, *69*, 168–180. [[CrossRef](#)]
44. Thomsen, K.J.; Murray, A.S.; Buylaert, J.P.; Jain, M.; Hansen, J.H.; Aubry, T. Testing single-grain quartz OSL methods using sediment samples with independent age control from the Bordes-Fitte rockshelter (Roches d’Abilly site, Central France). *Quat. Geochronol.* **2016**, *31*, 77–96. [[CrossRef](#)]
45. Nanson, G.C.; Price, D.M.; Jones, B.G.; Maroulis, J.C.; Coleman, M.; Bowman, H.; Cohen, T.J.; Pietsch, T.J.; Larsen, J.R. Alluvial evidence for major climate and flow regime changes during the middle and late Quaternary in eastern central Australia. *Geomorphology* **2008**, *101*, 109–129. [[CrossRef](#)]
46. Daley, J.; Croke, J.; Thompson, C.; Cohen, T.; Macklin, M.; Sharma, A. Late Quaternary channel and floodplain formation in a partly confined subtropical river, eastern Australia. *J. Quat. Sci.* **2017**, *32*, 729–743. [[CrossRef](#)]
47. Cohen, T.J.; Nanson, G.C.; Jansen, J.D.; Jones, B.G.; Jacobs, Z.; Treble, P.; Price, D.M.; May, J.-H.; Smith, A.M.; Ayliffe, L.K.; et al. Continental aridification and the vanishing of Australia’s megalakes. *Geology* **2011**, *39*, 167–170. [[CrossRef](#)]
48. McGowan, H.A.; Petherick, L.M.; Kamber, B.S. Aeolian sedimentation and climate variability during the late Quaternary in southeast Queensland, Australia. *Palaeogeogr. Palaeoclimatol. Palaeoecol.* **2008**, *265*, 171–181. [[CrossRef](#)]
49. Moss, P.T.; Tibby, J.; Petherick, L.; McGowan, H.; Barr, C. Late Quaternary vegetation history of North Stradbroke Island, Queensland, eastern Australia. *Quat. Sci. Rev.* **2013**, *74*, 257–272. [[CrossRef](#)]
50. Petherick, L.M.; Moss, P.T.; McGowan, H.A. An extended Last Glacial Maximum in subtropical Australia. *Quat. Int.* **2016**, *432*, 1–12. [[CrossRef](#)]
51. Reeves, J.M.; Barrows, T.T.; Cohen, T.J.; Kiem, A.S.; Bostock, H.C.; Fitzsimmons, K.E.; Jansen, J.D.; Kemp, J.; Krause, C.; Petherick, L.; et al. Climate variability over the last 35,000 years recorded in marine and terrestrial archives in the Australian region: An OZ-INTIMATE compilation. *Quat. Sci. Rev.* **2013**, *74*, 21–34. [[CrossRef](#)]
52. Petherick, L.M.; McGowan, H.A.; Moss, P.T.; Kamber, B.S. Late Quaternary aridity and dust transport pathways in eastern Australia. *Quat. Australas.* **2008**, *25*, 2–11.

53. Donders, T.H.; Wagner, F.; Visscher, H. Late Pleistocene and Holocene subtropical vegetation dynamics recorded in perched lake deposits on Fraser Island, Queensland, Australia. *Palaeogeogr. Palaeoclimatol. Palaeoecol.* **2006**, *241*, 417–439. [[CrossRef](#)]
54. McGowan, H.; Marx, S.; Moss, P.; Hammond, A. Evidence of ENSO mega-drought triggered collapse of prehistory Aboriginal society in northwest Australia. *Geophys. Res. Lett.* **2012**, *39*, L22702. [[CrossRef](#)]
55. Shulmeister, J.; Lees, B.G. Pollen evidence from tropical Australia for the onset of an ENSO-dominated climate at c. 4000 BP. *Holocene* **1995**, *5*, 10–18. [[CrossRef](#)]
56. Spratt, R.M.; Lisiecki, L.E. A Late Pleistocene sea level stack. *Clim. Past* **2016**, *12*, 1079–1092. [[CrossRef](#)]
57. Woolfe, K.L.; Larcombe, P.; Naish, T.; Purdon, R.G. Lowstand rivers need not incise the shelf: An example from the Great Barrier Reef, Australia, with implications for sequence stratigraphic models. *Geology* **1998**, *26*, 75–78. [[CrossRef](#)]
58. Lewis, S.E.; Sloss, C.R.; Murray-Wallace, C.V.; Woodroffe, C.D.; Smithers, S.G. Post-glacial sea-level changes around the Australian margin: A review. *Quat. Sci. Rev.* **2013**, *74*, 115–138. [[CrossRef](#)]
59. Daley, J.; Cohen, T. Climatically controlled river terraces in eastern Australia. *Quaternary* **2018**, *1*, 23. [[CrossRef](#)]
60. Croke, J.; Fryirs, K.; Thompson, C. Channel–floodplain connectivity during an extreme flood event: Implications for sediment erosion, deposition, and delivery. *Earth Surf. Process. Landf.* **2013**, *38*, 1444–1456. [[CrossRef](#)]
61. Croke, J.; Thompson, C.; Denham, R.; Haines, H.; Sharma, A.; Pietsch, T. Reconstructing a millennial-scale record of flooding in a single valley setting: The 2011 flood-affected Lockyer Valley, south east Queensland Australia. *J. Quat. Sci.* **2016**, *31*, 936–952. [[CrossRef](#)]

**Disclaimer/Publisher’s Note:** The statements, opinions and data contained in all publications are solely those of the individual author(s) and contributor(s) and not of MDPI and/or the editor(s). MDPI and/or the editor(s) disclaim responsibility for any injury to people or property resulting from any ideas, methods, instructions or products referred to in the content.